Optics and Laser Technology 119 (2019) 105634

Contents lists available at ScienceDirect

Optics and Laser Technology

journal homepage: www.elsevier.com/locate/optlastec

Full length article

CPT atomic clock with cold-technology-based vapour cell

S. Kobtsev[b,c], S. Donchenko[a], S. Khripunov[b,c], D. Radnatarov[b,c,*], I. Blinov[a], V. Palchikov[a]

[a] FSUE «All-Russian Scientific Research Institute of Physical-Technical and Radiotechnical Measurements» (FSUE «VNIIFTRI»), Russian Federation
[b] Tekhnoscan-Lab LLC, Russian Federation
[c] Novosibirsk State University, Russian Federation

HIGHLIGHTS

- All-direct-bonded Rb cells for highly stable mini atomic clocks is firstly reported.
- Applied fabrication technology is low-temperature in contrast to alternative ones.
- Proposed fabrication method provides perfect repeatability of cell parameters.
- Tests demonstrate competitive atomic clock stability at the 5×10^{-12} level over 1000 s.
- New vapour cell technology is compatible with a wide range of optical materials.

ARTICLE INFO

Keywords:
CPT atomic clock
Alkali vapour cell
Direct optical bonding
Buffer-gas mixture

ABSTRACT

Alkali-metal vapour cells are the core of coherent population trapping (CPT) atomic clocks, devices with a multitude of applications. These cells ensure high clock stability due to an atomic reference resonance. The contemporary technologies of alkali-metal vapour cells for atomic clocks compatible with mass production are relatively complicated and require special materials, as well as sub-technologies. The present work for the first time studies atomic CPT cocks with rubidium miniature cells fabricated with a simpler direct optical bonding technology, which has never hitherto been used for this purpose. The proposed technology can be implemented both in industrial and in laboratory setting. The measured stability of CPT atomic clock with rubidium cells fabricated with this technology amounted to 4×10^{-11} over 1 s and 1.3×10^{-12} over 10^3 s. The generated results indicate that the direct optical bonding technology can be successfully utilised for fabrication of compact cells with alkali-metal vapours for metrological and sensor applications.

1. Introduction

An alkali-metal vapour cell is the core of an atomic clock based on a coherent population trapping (CPT) resonance [1]. The recent demand for smaller atomic CPT clocks [2–5] and their mass production poses new demands on the technologies of miniaturised gas cells. The most important are requirements of repeatable CPT resonance parameters and the cell dimensions, as well as those of relatively long cell lifetime. At present, these requirements are met by the anodic bonding technology of miniature cell fabrication, which is thoroughly covered in recent reviews [6,7] on technologies alkali-metal vapour cell fabrication. Anodic bonding is a means of joining glass materials without glue based on electro-chemical processes taking place between joined surfaces at elevated temperatures and under action of electric field [8]. This process can be used for assembly of a gas cell by reliable gas-tight joining of two cell windows with a cylindrical body. One of the problems suffered by this fairly complex technology is the requirement of two special and different materials for the joined elements in order to ensure the necessary chemical reactions between their surfaces. At the same time, their thermal expansion coefficients have to be matched for minimisation of mechanical stress. In practice, there is only one pair of materials meeting these requirements, silicon and borosilicate glass. Therefore, the anodic bonding technology imposes a strict limit on the material choice. It is worth noting that anodic bonding technology also comprises sub-technologies that require specialised equipment. Among these sub-technologies are those for introduction of alkali metal into the cell, technologies of dicing an array of micro-cells into single cell units. In certain cases, they have to be supplemented by the technology of two-chamber cell fabrication, getter technology, and special coatings. Another significant demerit of anodic bonding is elevated temperature: the necessary chemical processes occur at 250–450 °C. Sealing the gas cell off at such high temperatures may result in release of oxygen from

* Corresponding author.
E-mail address: D.Radnatarov@gmail.com (D. Radnatarov).

https://doi.org/10.1016/j.optlastec.2019.105634
Received 25 March 2019; Received in revised form 27 May 2019; Accepted 10 June 2019

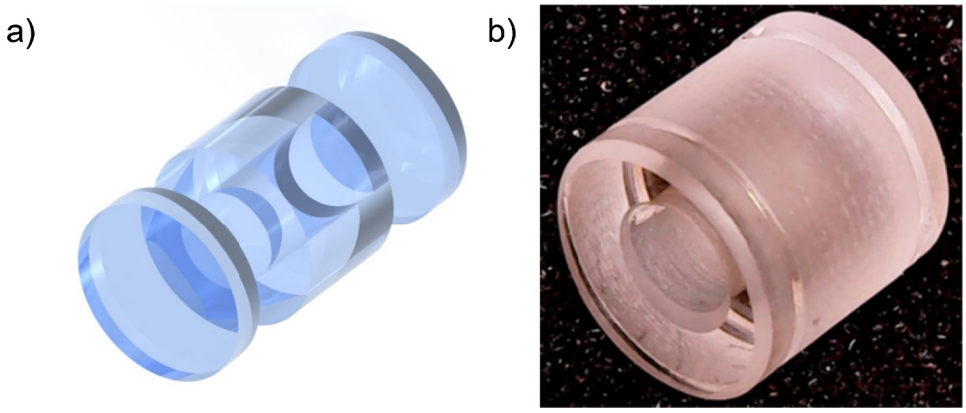

Fig. 1. Cold-technology-based vapour cell: (a) exploded 3D model of the cell elements, (b) photograph of an assembled cell.

the cell walls (both from silicon and glass), leading to oxidation of the cell agent (alkali metal). Various ways exist for minimisation of this effect [9], nevertheless, even this brief analysis demonstrates that the anodic bonding technology is far from being optimal for gas cell manufacture.

This work studies for the first time atomic CPT clocks using cells fabricated with a different simpler technology. Its primary advantages compared to anodic bonding are low process temperature (room temperature is sufficient) and possibility to use the same optical material for all joined parts (in our case, quartz). As our research demonstrates, optical cells fabricated according to this low-temperature technology provide highly competitive parameters of atomic CPT clocks.

2. Low-temperature technology of optical cell manufacture

2.1. Method description

We based our low-temperature cell fabrication technology on the well-known optical contact bonding method for glue-less joining of dielectric components [10–13]. When clean polished faces of such components are brought to about a nanometre apart, the molecular forces existing between hydroxyl groups of contact surfaces lead to reliable joining of these surfaces [14–21]. The bond is ensured by intermolecular forces and, unlike anodic bonding technology, is not accompanied by a chemical reaction. Optical contact bonding occurs at room temperature, and it is sufficient to press the surfaces against each other. This method poses more stringent requirements to the quality of polishing of the joined surfaces as compared to the anodic bonding method, which also makes use of electrostatic forces. The key conditions of good optical contact are high flatness and low roughness of the joined surfaces ($< \lambda/10$ peak-to-valley (PV) at $\lambda = 0.6$ μm [22,23] and λ–2λ correspondingly [24]), as well as their cleanness. Observation of these conditions allows durable and reliable optical component joins. In case when one or both joined surfaces are elastic and may deform in the process of joining [22] (for instance, relatively thin optical parts), the flatness requirement may be relaxed.

The bond strength of the join created *via* the direct optical bonding method amounts to ~0.1–0.25 J/m^2 [25] (referring to the work that must be expended in order to detach joined elements if their contact area equals 1 m^2) and may grow over time [26]. It can be also improved by thermal or mechanical post-processing [15,27]. In gas cell manufacture, durability of joins made with low-temperature optical contact is mostly important for sealing off the internal cell volume:

1. When individual cells are fabricated, it is necessary to keep the cell airtight both during mechanical manipulations (transportation, installation, possible vibrations) and when it is heated up to the working temperature (60–80 °C) [6].
2. When cell arrays are fabricated, it is also required that the cells remain air-tight in the process of array dicing into individual cells. This is a significant additional mechanical stress for the optical gas cells.

In the present work, we relied upon the technology of individual cell fabrication, therefore the requirements to the optical contact strength were not the highest.

It is also necessary to point out the following:

1. The cell elements may be made of a broad variety of optical materials. These materials must satisfy the above-listed requirements to their bonded surfaces, as well to the internal cell walls, which should not release any substances when heated up to the working temperature (as a rule, 60–80 °C);
2. Additionally the cell windows should be transparent to the radiation wavelength used for atomic clocks.

2.2. Cell design elements

In order to make a cell by direct optical bonding, we used three fused silica elements as shown in Fig. 1a: two identical windows having diameter of 8 mm and thickness of 1.5 mm, and a 5-mm long cylinder with the outside diameter 8 mm and internal bore of 4 mm. The cell elements were fabricated in a pilot optical facility. The surface finish quality corresponded to 20–10 Scratch-Dig (high-precision quality). Flatness of the joined optical surfaces of the cylindrical elements and the cell windows was controlled with a 3D laser surface profiler MII-4 M (LOMO) (Fig. 2a and b) and was measured within $\lambda/10$ PV. Fig. 2a presents the measured surface profile of the cell's central part (cylinder end), whereas Fig. 2b shows the measured surface profile of a cell window. Roughness of the optical surfaces of the cell elements was measured with an atomic-force microscope Bruker MultiMode 8 (Fig. 2c and d) and was within Ra $<$ 1 nm, where Ra is the mean of the absolute profile deviations along the base length. Measured parameters of the surfaces to be bonded demonstrate that their quality (flatness, roughness) satisfies the direct optical bonding requirements even when fabricated in a small optical workshop. Industrial production facilities with special polishing equipment [28] will ensure even higher surface quality.

Fabrication of optical cells by direct bonding was done as follows. First, one of the windows was direct-bonded to the cylinder. After that, the cell was placed inside a vacuum chamber, where ^{87}Rb was introduced into the cell cavity as a micro-droplet with a volume of ~1 μL. Then the vacuum chamber was filled with the buffer gas and the second cell window was bonded to the cylinder with the help of two vacuum manipulators to complete the cell. The cell assembly procedure was performed in general lab conditions with no access to commercial wafer

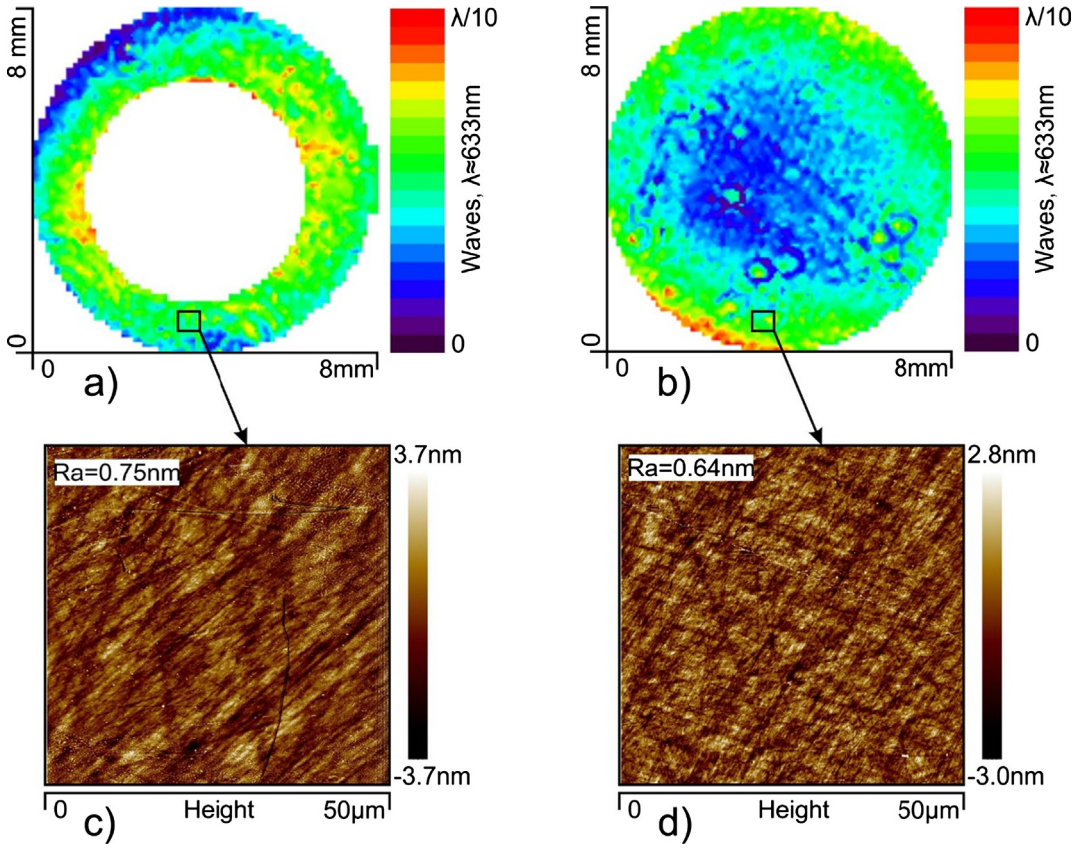

Fig. 2. (a), (c) surface of the cell central part (cylinder end); (b), (d) – surface of the cell window.

bonding equipment or to professional optical technicians.

Shown in Fig. 1b is a photograph of a cell fabricated according to the above-described technology. The process was conducted at room temperature and outside the vacuum chamber, the cell parts were manipulated in clean air corresponding to class 5 of the ISO 14644-1 standard [29]. In total, over 40 cells were made according to this technology, and to measure repeatability of their parameters, spectroscopic testing of the cells was carried out and stability of CPT atomic clocks using them was also measured.

3. Experiment

3.1. Installation layout

Spectroscopic parameters of the fabricated Rubidium gas cells, – absorption spectrum and CPT resonance contour, – were measured with the experimental set-up shown in Fig. 3. It used a single-frequency Vertical External Cavity Surface Emitting Laser (VECSEL) emitting at around 795 nm, which corresponds to the D1 absorption line in ^{87}Rb. It had linewidth of 50 MHz, output power of 50 μW and beam diameter of 2 mm. The laser's output wavelength could be continuously tuned by adjusting laser injection current (0.6 nm/mA) or the laser temperature (0.06 nm/K). For elimination of the external magnetic fields, the optical cell was enclosed into a 3-layer μ-metal magnetic shield. Inside the shield, a pair of Helmholtz coils were used to create a 100 mG field parallel to the direction of radiation propagation, in order to split Zeeman sub-levels of the ^{87}Rb ground state. The cell temperature was stabilised by keeping constant the temperature of the magnetic shield housing the cell. This ensured high uniformity of the cell temperature, which was stabilised to the precision of several mK for a set value in the range of 60 to 80 °C. Fig. 4a demonstrates a typical measured transmission spectrum of a fabricated cell around the D1 line at the cell

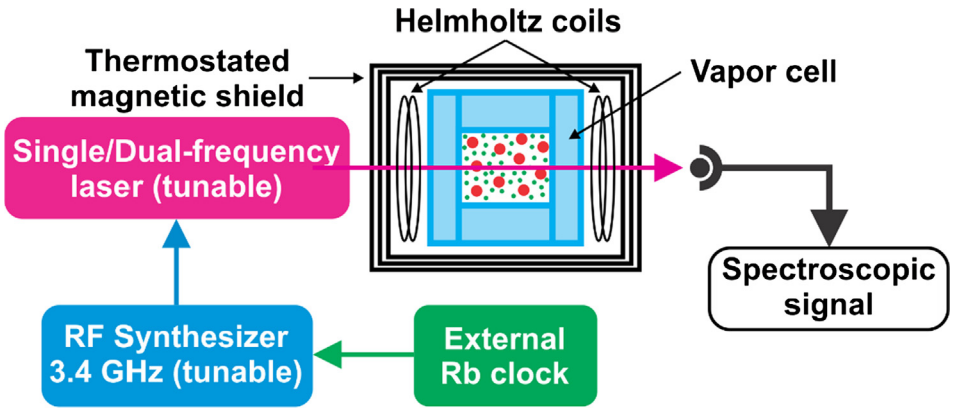

Fig. 3. The experimental set-up layout for measurement of absorption spectra and the CPT resonance shape.

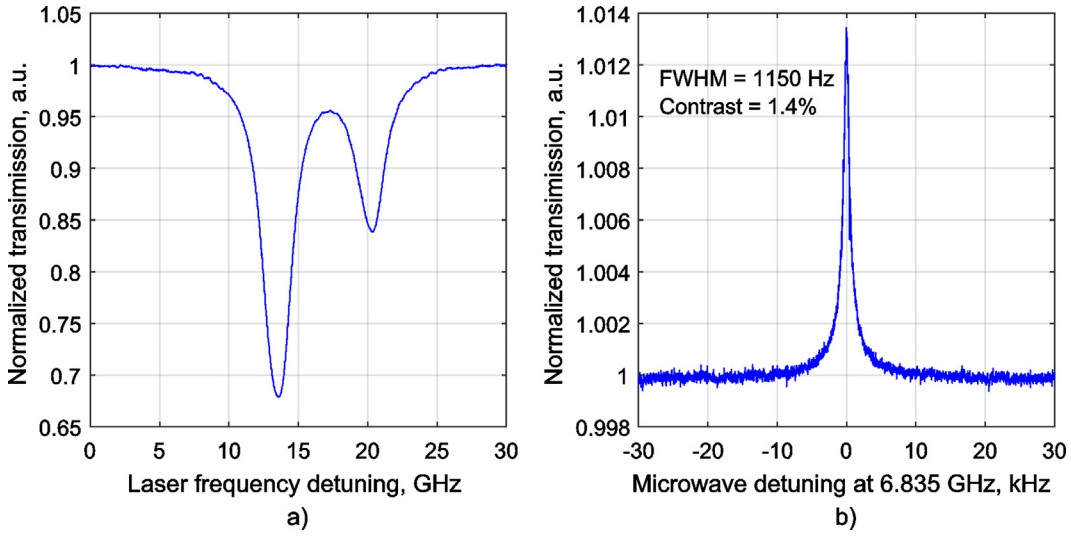

Fig. 4. (a) Rb D1 absorption lines observed when passing laser light through the cell, (b) CPT resonance line in the Rb-Ar/N_2 fabricated cell heated to 70.5 °C.

temperature of 70.5 °C. The spectrum prominently features absorption peaks corresponding to $5^2S_{1/2} \rightarrow 5^2P_{1/2}$ transitions of the ^{87}Rb atom and spaced 6.835 GHz apart.

For measurement of the CPT resonance profile, the input laser polarisation was transformed into circular with a λ/4 plate, in order to excite a coherent state between the magneto-insensitive sub-levels of the ^{87}Rb ground-state. Laser injection current was modulated at the frequency equal to 1/2 of the ground-state hyperfine resonance frequency of ^{87}Rb (3.417 GHz). This led to emergence in the laser output spectrum of optical sidebands with a 6.835-GHz frequency difference. When these sidebands interacted with the three state Λ–configuration of the D1 line having two hyperfine ground states and the sideband frequency difference was swept around 6.835 GHz, a CPT resonance was formed. In order to measure precisely the CPT resonance profile, we used an external Rb frequency reference with instability within 4×10^{-12} over 1 s. Fig. 4b gives a typical measured CPT resonance contour with a 1.15-kHz width and contrast (the amplitude-to-background ratio) of 1.4%. It is necessary to mention that the measured parameters of CPT resonances in (FWHM and contrast) in the fabricated cells are similar to those reported for other buffer-gas cells manufactured differently [30–35].

The width and contrast of a CPT resonance determine the accuracy of locking the oscillator frequency onto its peak, and the short-term (over 1 s) stability of an atomic clock depends on this accuracy. Longer-term stability is governed by the stability of the CPT resonance position, which, in turn, depends on stability of its excitation and detection parameters, as well as on stability of the ambient conditions (temperature, magnetic field, etc.). For example, the cell temperature may affect impact shift of the CPT resonance. For minimisation of this shift, a two-component buffer gas is often used [36,37]. In our experiments, we used a buffer gas containing a mix of argon and nitrogen with partial pressure ratio of $P_{Ar}/P_{N2} \sim 1.4$ and total pressure of 80 torr. Given in Fig. 5 is the dependence of CPT resonance shift upon the cell temperature. As indicated, the temperature shift is minimised in the vicinity of 70.5 °C. This temperature was chosen as the working point in subsequent metrological testing.

The stability of CPT atomic clocks with the fabricated cells was measured in the experimental set-up of Fig. 6, similar to the ones discussed earlier in [38,39].

In this experiment, both the short- (over 1 s) and long-term (over 10^3 s) CPT atomic clock stability was measured. Servo system based on National Instruments' PXI created the feed-back necessary for locking frequency of the local oscillator (temperature-compensated quartz crystal oscillator TCVCXO, IQD FOQ GmbH) onto the CPT resonance.

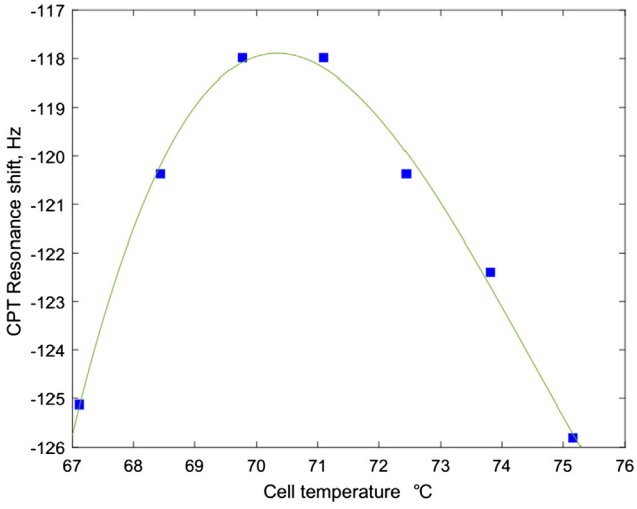

Fig. 5. Dependence of the CPT resonance position upon the cell temperature.

Microwave frequency (3.417 GHz) was swept at 2 kHz, and the error signal was registered with a phase-lock detector at this frequency. An additional feed-back loop was used to stabilise the laser wavelength at the centre of the Doppler contour. For this, the laser injection current was additionally modulated at 10.1 kHz. It should be mentioned here that the laser output wavelength was stabilised by using the same cell, and not an external reference one, as it was done, for instance, in [40].

The frequency instability measurement was done with a frequency comparator by comparing the measured frequency to that of the Rb reference with internal frequency instability not exceeding 10^{-13} over 1 s. Fig. 7 presents a typical experimental dependence of the Allan deviation upon time for a CPT atomic clock with one of the fabricated cells. Short-term instability was equal to 4×10^{-11} over 1 s and further on during the 1–1000-second period, it was dropping approximately as $t^{-1/2}$, and amounted to 1.3×10^{-12} over 1000 s. The recorded stability figures are similar to those measured earlier in the same installation, but with cells made by glass-blowing technology [38]. Comparing stability of CPT atomic clock with cold-technology-based vapour cells to that of other clocks using cells fabricated by anodic bonding technique is not entirely correct, since the clock stability is governed not only by the cell parameters, but also by properties of other clock components, which may differ significantly. Nevertheless, in general, stability of CPT atomic clock with cold-technology-based vapour cell is of the same

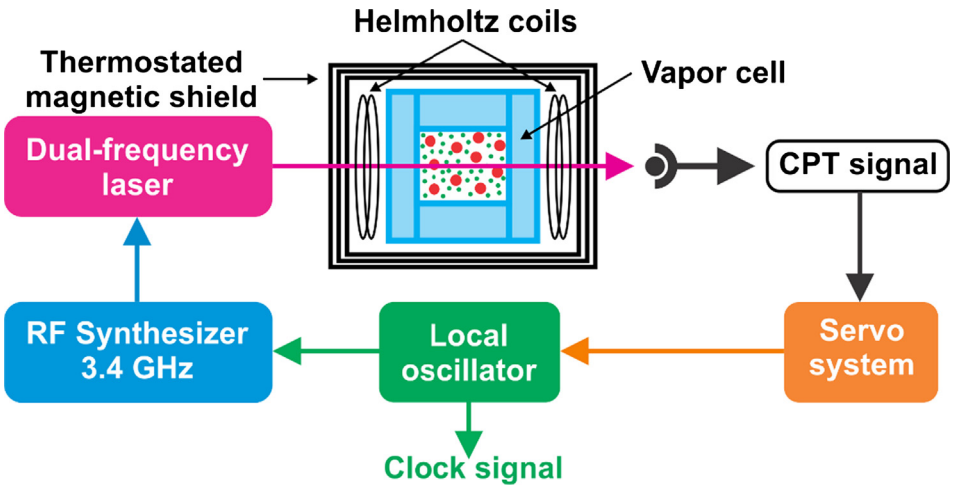

Fig. 6. Experimental installation for measurement of stability of atomic CPT clocks using the fabricated cells.

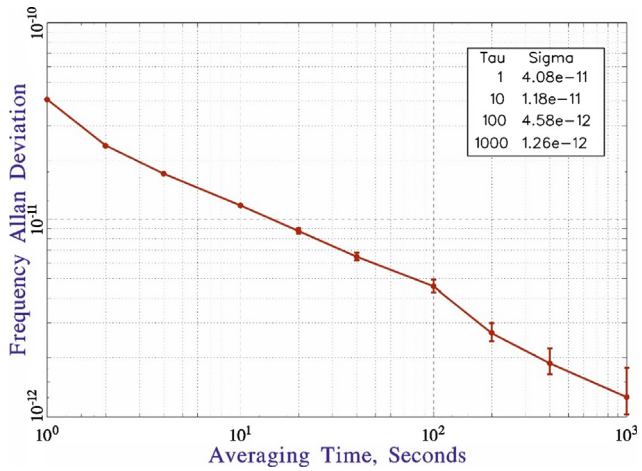

Fig. 7. Typical Allan deviation of the CPT atomic clock using the fabricated cell.

order as that of similar clocks relying on same-sized cells fabricated by anoding bonding [6].

3.2. Repeatability of spectral parameters of cells

Testing of spectral parameter repeatability was carried out on a batch of 42 cells fabricated according to the technology explained earlier on. For all the cells, the width and contrast of the CPT resonance were measured, as well as short-term (over 1 s) instability of atomic clock using each of the tested cells. The obtained results are presented in Fig. 8. Red curve is data approximation with a normal distribution. It can be seen that variability of the CPT resonance width lie within the 1–2 kHz range with the distribution maximum at 1.55 kHz. The centre of the CPT resonance contrast distribution corresponds to 1.9% at variability range of 1.2–2.8%. The short-term instability of atomic clocks varies between 3.0×10^{-11} and 4.6×10^{-11} with a distribution maximum at 3.9×10^{-11}.

The results of the 42-cell batch testing indicate good parameter repeatability of the cells fabricated according to the proposed low-temperature technology. The relatively narrow spread is, likely, due to small variation of the buffer gas pressure from cell to cell, because each cell was filled with buffer gas individually.

3.3. Problem of non-uniform cell heating

Using optical cells in atomic clocks implies heating them up to the working temperature in the range of 60–80 °C in order to vaporise the alkali metal and to make them dense enough for generation of the optimal CPT signal and to ensure minimal drift of the CPT resonance [36]. When the cell is not heated uniformly, rubidium vapour condensates on colder parts of the cell. Non-uniform cell heating may also exacerbate temperature sensitivity of the clock frequency [41]. It is difficult to ensure temperature uniformity in all parts of the cell. The coldest locations usually happen to be windows, which must be open for laser radiation passing through. If that is the case, the window transmittance may drop off with time because of rubidium deposition, which has a negative impact on the atomic clock parameters. One of clever solutions to this problem is placement of the cell heating coil directly on the cell windows [42]. This leads to the windows having higher temperature than the rest of the cell. In ultra-small cells and relatively thin windows, this ensures proper heating of the entire cell and a downward temperature gradient towards the cell interior.

A combined approach against rubidium deposition on the windows is also possible when overall cell heating is provided by an external element and the window heaters are only used to ensure their higher temperature compared to the rest of the cell.

For testing of this approach, we used sputtering through a mask to deposit conductive heaters on the windows. They were designed as bifilar structures for minimisation of magnetic field created by the heating current. The technology proposed in [43] was used to make ~200-nm thick indium-tin oxide (ITO) conductors transparent to the 795-nm radiation. Each deposited structure had resistance of 24 kΩ. Photographs of cell windows with the deposited heating elements are given in Fig. 9. Also shown in Fig. 9b is a miniature temperature sensor installed on the window surface, which was used to control the window cell temperature.

The dependence of temperature increase upon the voltage supplied to the deposited conductive structure is shown in Fig. 10. It can be seen that a temperature difference of 1 °C requires 14 V, corresponding to energy consumption of one window heater around 8 mW, which is an acceptable figure for many compact atomic clocks. Two accompanying circumstances should be also mentioned:

1. Our experiments were carried out in air, leading to higher heat dissipation from the cell windows (compared to vacuum, for instance). Therefore, in vacuum, the same positive temperature difference between the windows and the rest of the cell will require substantially less energy;
2. The positive temperature difference between the cell windows and

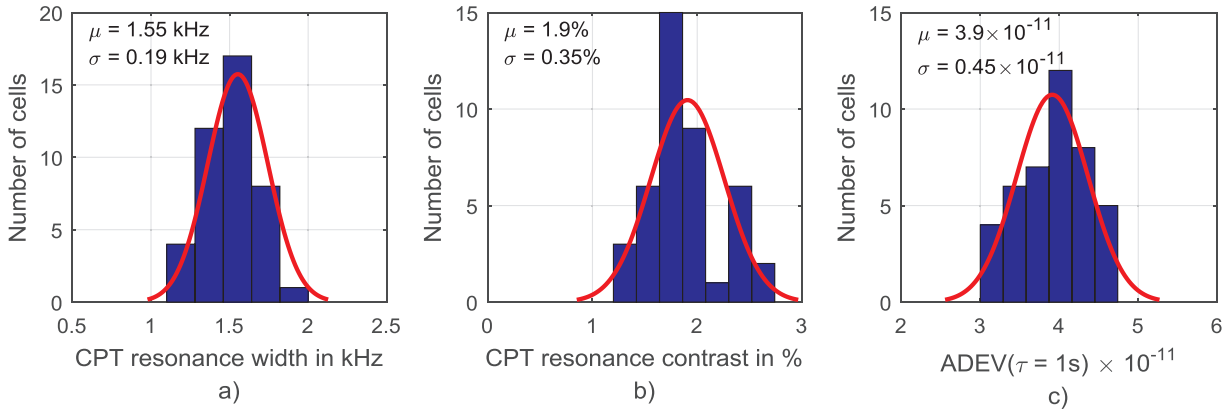

Fig. 8. Statistical distribution of results among the 42 tested cells: (a) CPT resonance width; (b) CPT resonance contrast; (c) short-term atomic clock instability.

the rest of the cell may be significantly lower than 1 °C. It may be sufficient to keep it at 0.1 °C or even lower.

Considering these points, in an evacuated atomic clock chamber, the proposed heating element will consume less than 1 mW.

4. Conclusion

The conducted research has shown that direct optical bonding can definitely be used as a key technology for manufacture of alkali-metal vapour cells for atomic CPT clocks. The proposed and tested technology is universal and may be used to create millimeter-scale size atomic MEMS cells both in mass production and in laboratory facilities. It is an important advantage of direct optical bonding that it does not require special equipment for joining cell elements and is compatible with a variety of optical materials to be used for cell fabrication, while allowing all elements to be made of the same material (for example, quartz).

A batch of over 40 fabricated cells are an evidence of comparatively high repeatability of the cell parameters: the CPT resonance width and contrast of 1–2 kHz and 1.2–2.8% respectively; short-term atomic clock stability of (3.0…4.6) × 10^{-11}, and long-term stability of 1.3 × 10^{-12} over 103 s.

In the proposed technology, we directly introduced an alkali metal (Rb) into the cell, although the same approach can be used with alkali-metal compounds, such as RbN_3 or CsN_3 [31,42] followed by UV photo-decomposition of the compound through the quartz window of the cell. Through quartz, UV photo-decomposition is significantly more efficient than, for instance, through borosilicate glass suffering from much higher UV absorption. The proposed technology is equally compatible with introduction of the alkali metal into the cell as a dispensing pill [44] and subsequent extraction of the alkali metal by local laser heating.

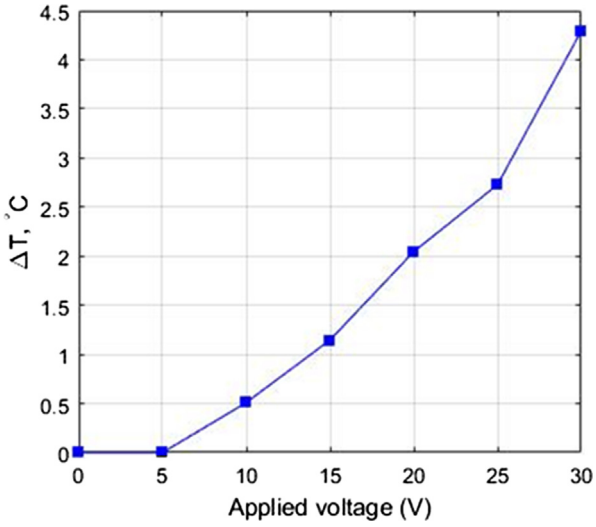

Fig. 10. Dependence of the cell window temperature elevation relative to the rest of the cell upon the voltage applied to the conductive window heater.

Among drawbacks of the proposed direct optical bonding technology one can mention that low-temperature joins remain detachable. For example, joined parts may be separated by non-uniform heating of the join surface with relatively high temperature gradient (> 100 °C). The combination of direct optical bonding with heating [23,45] allows permanent joins. This, however, is not necessary for atomic clocks, since the optical cell is heated uniformly and kept at a relatively low

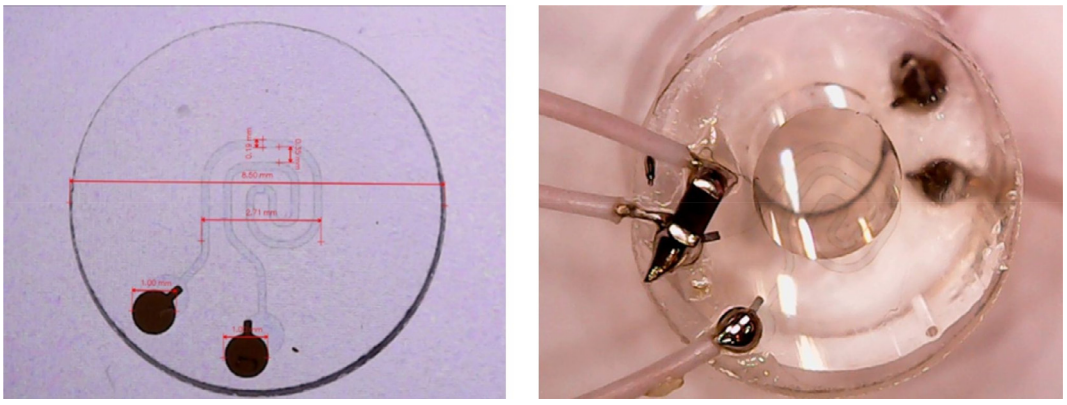

Fig. 9. Photographs of the cell windows with deposited conductive heating elements.

temperature (60–80 °C).

In general, the presented results indicate a high potential of the proposed technology for further development of atomic clocks in order to make them more cost-effective and broadly available.

Acknowledgments

The work was supported by the contract of the Ministry of Industry and Trade of the Russian Federation and the grant of the Ministry of Science and Higher Education of the Russian Federation (3.889.2017/PCH).

References

[1] J. Vanier, Atomic clocks based on coherent population trapping: a review, Appl. Phys. B 81 (4) (2005) 421–442.
[2] S. Knappe, V. Shah, P.D.D. Schwindt, L. Hollberg, J. Kitching, L.-A. Liew, J. Moreland, A microfabricated atomic clock, Appl. Phys. Lett. 85 (9) (2004) 1460–1462.
[3] D.W. Youngner, L.M. Lust,D.R. Carlson, S.T. Lu, L.J. Forner, H.M. Chanhvongsak, T. D. Stark, A manufacturable chip-scale atomic clock, in: TRANSDUCERS 2007–2007 Int. Solid-State Sensors, Actuators and Microsystems Conf., Lyon, 2007, pp. 39–44.
[4] A. Godone, F. Levi, C.E. Calosso, S. Micalizio, High-performing vapor-cell frequency standards, Riv. Nuovo Cimento 38 (2015) 133–171.
[5] P. Cash, W. Krzewick, P. Machado, K.R. Overstreet, M. Silveira, M. Stanczyk, D. Taylor, X. Zhang, Microsemi Chip Scale Atomic Clock (CSAC) technical status, applications, and future plans, in: European Frequency and Time Forum (EFTF), Turin, 2018, pp. 65–71.
[6] J. Kitching, Chip-scale atomic devices, Appl. Phys. Rev. 5 (2018) 031302.
[7] P. Knapkiewicz, Technological assessment of MEMS alkali vapor cells for atomic references, Micromachines 10 (1) (2019) 25.
[8] A.C. Lapadatu, K. Schjolberg-Henriksen, Anodic bonding, in: P. Ramm, J. Lu, M. Taklo (eds.), Chapter 4 in book “Handbook of Wafer Bonding”, Wiley-VCH Verlag, 2012.
[9] B.J. Todd, Outgassing of glass, J. Appl. Phys. 26 (10) (1955) 1238–1243.
[10] L. Rayleigh, A study of glass surfaces in optical contact, Proc. R. Soc. Lond. A Math. Phys. Sci. 156 (888) (1936) 326–349.
[11] R.B. Holt, Research on optical contact bonding, Device Development Corp., 1966 54p.
[12] A. Ploessl, G. Krauter, Wafer direct bonding: tailoring adhesion between brittle materials, Mater. Sci. Eng. R Rep. 25 (1–2) (1999) 1–88.
[13] J. Haisma, G. Spierings, Contact bonding, including direct-bonding in a historical and recent context of materials science and technology, physics and chemistry: historical review in a broader scope and comparative outlook, Mater. Sci. Eng. R. Rep. 37 (1–2) (2002) 1–60.
[14] D. Ando, K. Oishi, T. Nakamura, S. Umeda, Glass direct bonding technology for hermetic seal package, Proc. IEEE (1997) 186–190 ISBN 0-7803-3744-1.
[15] S.H. Christiansen, R. Singh, U. Gosele, Wafer direct bonding: From advanced substrate engineering to future applications in micro/nanoelectronics, Proc. IEEE. 94 (12) (2006) 2060–2106.
[16] J. Haisma, N. Hattu, J.T. Pulles, E. Steding, J.C. Vervest, Direct bonding and beyond, Appl. Opt. 46 (27) (2007) 6793–6803.
[17] C. Ventosa, F. Rieutord, L. Libralesso, C. Morales, F. Fournel, H. Moriceau, Hydrophilic low-temperature direct wafer bonding, J. Appl. Phys. 104 (2008) 123524.
[18] M. Eichler, B. Michel, P. Henneke, M. Gabriel, C.P. Klages, Low-temperature direct bonding of Borosilicate, Fused Silica and Functional Coatings, ECS Trans. 33 (4) (2010) 339–348.
[19] G. Kalkowski, S. Risse, C. Rothhardt, M. Rohde, R. Eberhardt, Optical contacting of low-expansion materials, Proc. SPIE 8126 (2011) 81261F.
[20] T. Mizumoto, Y. Shoji, R. Takei, Direct wafer bonding and its application to waveguide optical isolators, Materials (Basel) 5 (5) (2012) 985–1004.
[21] K. Henttinen, T. Suni, Silicon direct bonding. Chapter 29 in book “Handbook of Silicon Based MEMS Materials and Technologies (Second Edition)”, Elsevier, Series: Micro and Nano Technologies, 2015, p. 591–598.
[22] Q.-Y. Tong, U. Gosele, Thickness considerations in direct silicon wafer bonding, J. Electrochem. Soc. 142 (11) (1995) 3975–3979.
[23] G. Kalkowski, S. Risse, U. Zeitner, F. Fuchs, R. Eberhardt, A. Tünnermann, Glass-glass direct bonding, ECS Trans. 64 (5) (2014) 3–11.
[24] N. Miki, S.M. Spearing, Effect of nanoscale surface roughness on the bonding energy of direct-bonded silicon wafers, J. Appl. Phys. 94 (2003) 6800–6806.
[25] G.A.C.M. Spierings, J. Haisma, T.M. Michelsen, Surface-related phenomena in the direct bonding of silicon and fused-silica wafer pairs, Philips Res. Rep. 49 (1–2) (1995) 47–63.
[26] N.V. Tikhmenev, S.A. Zakurnaev, A.V. Ozarenko, V.S. Bystritsky, S.A. Myagkov, R.A. Stolyarov, K.E. Chechetov, S.E. Korshunov, Influence of surface treatment and purification methods of CO-115M glass-ceramics on optical contact strength, Sci. Tech. J. Inf. Technol. Mech. Opt. 16 (4) (2016) 613–619.
[27] H. Moriceau, F. Rieutord, F. Fournel, Y. Tiec, L. Cioccio, C. Morales, A. Charvet, C. Deguet, Overview of recent direct wafer bonding advances and applications, Adv. Nat. Sci.: Nanosci. Nanotechnol. 1 (2010) 043004.
[28] R. Komanduri, D.A. Lucca, Y. Tani, Technological advances in fine abrasive processes, CIRP Ann. 46 (2) (1997) 545–596.
[29] ISO, EN. 14644-1. Cleanrooms and associated controlled environments - Part 1: Classification of air cleanliness. European Standard, 1999.
[30] S. Knappe, V. Gerginov, P.D. Schwindt, V. Shah, H.G. Robinson, L. Hollberg, J. Kitching, Atomic vapor cells for chip-scale atomic clocks with improved long-term frequency stability, Opt. Lett. 30 (18) (2005) 2351–2353.
[31] L.A. Liew, J. Moreland, V. Gerginov, Wafer-level filling of microfabricated atomic vapor cells based on thin-film deposition and photolysis of cesium azide, Appl. Phys. Lett. 90 (11) (2007) 114106.
[32] R. Lutwak, A. Rashed, M. Varghese, G. Tepolt, J. LeBlanc, M. Mescher, D.K. Serkland, K.M. Geib, G.M. Peake, S. Römisch, The chip-scale atomic clock-prototype evaluation, in: Proc. 39th Annual Precise Time and Time Interval Meeting, Long Beach, California, 2007, pp. 269–290.
[33] Y. Pétremand, C. Schori, R. Straessle, G. Mileti, N. Rooij, P. Thomann, Low temperature indium-based sealing of microfabricated alkali cells for chip scale atomic clocks, in: EFTF-2010 24th European Frequency and Time Forum, Noordwijk, 2010, p. 1–3.
[34] S.M. Ignatovich, V.I. Vishnyakov, A.O. Makarov, M.N. Skvortsov, N.L. Kvashnin, V. A. Vasiliev, S.N. Atutov, D.V. Brazhnikov, V.I. Yudin, A.V. Taichenachev, S.N. Bagayev, CPT atomic clock based on an antirelaxation-coated cell and quadrature-signal method of the light shift cancellation, in: 2018 European Frequency and Time Forum (EFTF), Turin, 2018, pp. 83–86.
[35] R. Vicarini, V. Maurice, M.A. Hafiz, J. Rutkowski, C. Gorecki, N. Passilly, L. Ribetto, V. Gaff, V. Volant, S. Galliou, R. Boudot, Demonstration of the mass-producible feature of a Cs vapor microcell technology for miniature atomic clocks, Sens. Actuators A Phys. 280 (280) (2018) 99–106.
[36] J. Vanier, R. Kunski, N. Cyr, J.Y. Savard, M. Têtu, On hyperfine frequency shifts caused by buffer gases: application to the optically pumped passive rubidium frequency standard, J. Appl. Phys. 53 (8) (1982) 5387–5391.
[37] C. Affolderbach, F. Droz, G. Mileti, Experimental demonstration of a compact and high-performance laser-pumped rubidium gas cell atomic frequency standard, IEEE Trans. Instrum. Meas. 55 (2) (2006) 429–435.
[38] S. Khripunov, D. Radnatarov, S. Kobtsev, Atomic clock based on a coherent population trapping resonance in ^{87}Rb with improved high-frequency modulation parameters, Proc. SPIE 9378 (2015) 93780A.
[39] S. Kobtsev, D. Radnatarov, S. Khripunov, I. Popkov, V. Andryushkov, T. Steshchenko, V. Lunin, Y. Zarudnev, Feedback-controlled and digitally processed coherent population trapping resonance conversion in ^{87}Rb vapour to high-contrast resonant peak, New J. Phys. 19 (4) (2017) 043016.
[40] P. Yun, F. Tricot, C.E. Calosso, S. Micalizio, B. François, R. Boudot, S. Guérandel, E. Clercq, High-performance coherent population trapping clock with polarization modulation, Phys. Rev. Appl. 7 (2017) 014018.
[41] C.E. Calosso, A. Godone, F. Levi, S. Micalizio, Enhanced temperature sensitivity in vapor-cell frequency standards, IEEE Trans. Ultrason. Ferroelectr. Freq. Control 59 (12) (2012) 2646–2654.
[42] T. Overstolz, J. Haesler, G. Bergonzi, A. Pezous, P.A. Clerc, S. Ischer, J. Kaufmann, M. Despont, Wafer scale fabrication of highly integrated rubidium vapor cells, in: 2014 IEEE 27th Int. Conf. on Micro Electro Mechanical Systems (MEMS), San Francisco, CA, 2014, pp. 552–555.
[43] A. Surtaev, V. Serdyukov, J. Zhou, A. Pavlenko, V. Tumanov, An experimental study of vapor bubbles dynamics at water and ethanol pool boiling at low and high heat fluxes, Int. J. Heat Mass Transfer 126 (126) (2018) 297–311.
[44] Z.L. Newman, V. Maurice, T. Drake, J.R. Stone, T.C. Briles, D.T. Spencer, C. Frederick, Q. Li, D. Westly, B.R. Ilic, B. Shen, M.-G. Sun, K.Y. Yang, C. Johnson, D.M. Johnson, L. Hollberg, K.J. Vahala, K. Srinivasan, S.A. Diddams, J. Kitching, S.B. Papp, M.T. Hummon, Architecture for the photonic integration of an optical atomic clock, Optica 6 (5) (2019) 680–685.
[45] U. Gösele, Q.Y. Tong, Semiconductor wafer bonding, Annu. Rev. Mater. Sci. 28 (1) (1998) 215–241.